

Flow and Heat Transfer in Serpentine Channels

Chaitanya M. Karale

Industrial Flow Modeling Group, National Chemical Laboratory, Pune 411008, India

Dept. of Chemical Engineering, Institute of Chemical Technology, Mumbai 400019, India

Sunil S. Bhagwat

Dept. of Chemical Engineering, Institute of Chemical Technology, Mumbai 400019, India

Vivek V. Ranade

Industrial Flow Modeling Group, National Chemical Laboratory, Pune 411008, India

DOI 10.1002/aic.13954

Published online November 26, 2012 in Wiley Online Library (wileyonlinelibrary.com).

Serpentine channels are often used in microchannel reactors and heat exchangers. These channels offer better mixing, higher heat and mass-transfer coefficients than straight channels. In the present work, flow and heat transfer experiments were carried out with a serpentine channel plate comprising of 10 units (single unit dimensions: $1 \times 1.5 \text{ mm}^2$ in cross section, length 46.28 mm, D_h 1.2 mm) in series. Pressure drop and heat-transfer coefficients were experimentally measured. Flow and heat transfer in the experimental set-up were simulated using computational fluid dynamics (CFD) models to understand the mechanisms responsible for performance enhancement. The CFD methodology, thus, developed was applied to understand the effect of various geometrical parameters on heat transfer enhancement. A criterion was defined for evaluation of heat transfer performance (heat transfer per unit pumping power), thus, ensuring due considerations to required pumping power. The effect of geometrical parameters and the corresponding mechanisms contributing for enhancement are discussed briefly. Based on the results, a design map comprising different serpentine channels showing heat transfer enhancement with pumping power was developed for Reynolds number of 200 which will be useful for further work on flow and heat transfer in serpentine channels. © 2012 American Institute of Chemical Engineers AIChE J, 59: 1814–1827, 2013

Keywords: serpentine, pressure drop, heat transfer, computational fluid dynamics

Introduction

In the recent years, there is growing interest among the researchers for developing different microchannel reactors.^{1,2} Usually laminar flow regime prevails in such microchannel reactors. Laminar flow and development of boundary layers (velocity as well as thermal) reduce heat and mass transfer performance of such microreactors. One of the ways of overcoming this limitation is by breaking/disrupting boundary layer along with radial mixing. Various types of active and passive mixers are used for this purpose. Active mixers use external forces or power to achieve desired mixing. Passive devices use geometrical configuration for realizing desired mixing. Serpentine channel configurations are one of the popular choices of enhancing mixing.

The serpentine channel consists of a bend section with repeating units. Figure 1a shows simple schematic of a serpentine channel. A typical serpentine configuration can be classified in two broad categories (1) smooth bend (see Figure 1b) and (2) sharp bend (see Figure 1c). A typical serpentine channel as shown in Figure 1a can be specified using

the following parameters (a) bend angle (θ) (b) straight length before bend (L) or distance between the bends ($2L$) (c) radius of curvature at bend section (R_c), and (d) amplitude of the serpentine configuration (A). Based on the combinations of these four parameters, number of different serpentine configurations can be designed. The performance, in terms of pressure drop and heat transfer, will be different for different configurations. Therefore, in such cases, selection of geometrical configuration/parameters becomes a difficult task. Some examples of the serpentine configurations (sinusoidal channel, saw tooth configuration, etc.) are shown in Figures 1b, c.

This manuscript deals with a question of which serpentine configuration gives the best performance (maximum heat transfer performance at lowest power consumption). In this context, some of the published work is briefly reviewed here. In light of this review, attempt is made to quantify this issue computationally in the present work. Computational model and obtained results are discussed in the following sections.

Review of Previous Work

Single-phase laminar flow and heat transfer in serpentine channels were numerically studied by several authors^{2–9,10,11} to understand the effect of various geometrical parameters

Correspondence concerning this article should be addressed to V. V. Ranade at vv.ranade@ncl.res.in.

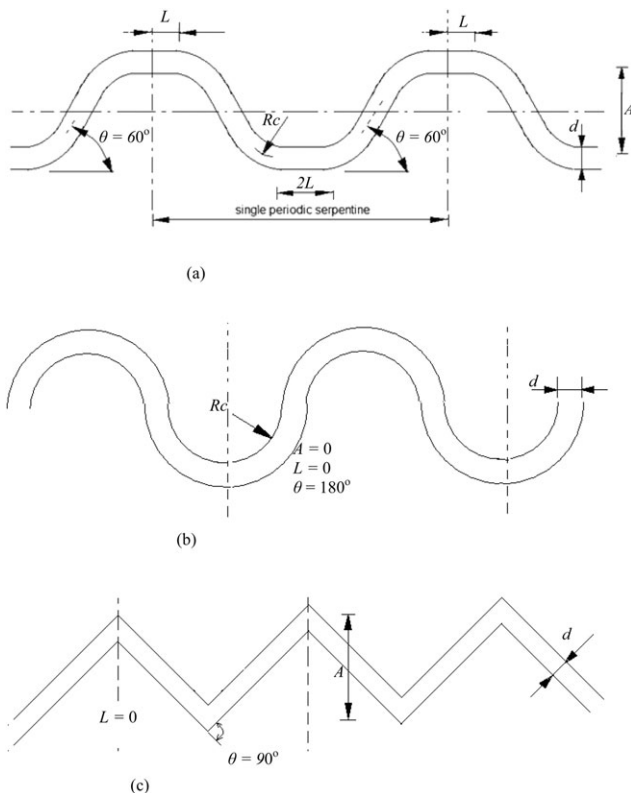


Figure 1. (a) Schematic of general serpentine channel; (b) schematic of sinusoidal serpentine channel; (c) schematic of saw-tooth configuration serpentine channel.

and operating conditions on pressure drop and heat transfer. The typical cross sections under the considerations were rectangular,^{3,4,7,9} circular,^{5,6,11} and semicircular ones.^{8,10,11} Compared to numerical efforts, the literature in terms of experimental data on single-phase flow characteristics in the channels with serpentine bends in the past is very limited.¹² In all the studies, with serpentine channels, significant heat transfer enhancements relative to straight pipe was found with the greater effect for $Pr > 1$. Some of the key published studies are summarized in Table 1.

The secondary flow structure present at the bend section helps to increase the rate of heat transfer by disrupting the thermal boundary layer. In published literature,^{3,5-8,10,11} ratios of Nusselt numbers, friction factors, or some combination of these were used to analyze the performance of the serpentine

channel $\left(\frac{Nu_{\text{serpentine}}}{Nu_{\text{straight}}} \text{ and/ or } \frac{f_{\text{serpentine}}}{f_{\text{straight}}} \text{ and/ or } \frac{Nu_{\text{serpentine}}}{f_{\text{serpentine}}} \frac{f_{\text{straight}}}{Nu_{\text{straight}}} \right)$.

These criteria do not directly indicate impact on effective heat transfer realized in these systems. Therefore, in this work, following additional criteria was used

$$\text{Performance enhancement} = \frac{(Q/PP)_{\text{Serpentine}}}{(Q/PP)_{\text{Straight channel}}} \quad (1)$$

where, Q is total rate of heat transfer and PP is pumping power. In the present study, total length of all serpentine configurations was kept constant; therefore, the denominator remains fixed value for a particular Re . Thus, above criterion provides a guideline for selecting configuration of a serpentine channel with respect to heat transfer enhancement per unit required pumping power over a straight channel.

In the present work, some experimental measurements of pressure drop and heat-transfer coefficient in a serpentine geometry were carried out and compared with the simulated results. The verified computational fluid dynamics (CFD) model, and simulations were then used to understand and to quantify influence various geometrical parameters on heat transfer performance of serpentine channel. These results are discussed in the following.

Flow and Heat Transfer in Serpentine Channel

CFD simulations

CFD simulations were carried out by using commercial code of Fluent 6.3.36 (of Fluent Inc.) and geometries were generated using Gambit 2.4 (of Fluent Inc.). The geometry used in the present CFD analysis consists of rectangular single serpentine channel having dimensions $1 \times 1.5 \times 46.28 \text{ mm}^3$ (aspect ratio H/W equal to 1.5). The configuration of the present serpentine channel involves smooth bend having bend angle of 180° , radius of curvature of 1.5 mm, zero straight length portion between bends, and amplitude of 20 mm. The computational domain is shown in Figure 2. The entire solution domain was meshed using hexahedral map elements. Grid sensitivity analysis was carried out and a computational grid of $30 \times 30 \times 500$ cells (single periodic serpentine) was found to be an appropriate choice. The channel width and height was meshed with double successive ratio of 1.1, whereas channel length was meshed with a double successive ratio of 1.02. Total 450,000 cells were used in the simulations.

Steady-state solutions for flow and heat transfer in serpentine channel for the Re range of 133–666 were obtained. The physical properties of the working fluid were constant with Prandtl number (Pr) of 6.97 (i.e., water). Solutions were obtained for the periodic case which represents periodically developed conditions in velocity as well as in temperature. The inlet temperature of the fluid was set at 300 K. The flow and energy equations were discretized using second-order upwind scheme. Appropriate under-relaxation factors were used for flow and energy equations. The SIMPLE algorithm was used for handling velocity–pressure coupling. Appropriate convergence criteria (residuals of continuity $< 1 \times 10^{-9}$ and of energy $< 1 \times 10^{-10}$) were used.

CFD simulations were carried out (with constant wall temperature of 373 K and adiabatic top wall) to quantify total heat transfer from the wall to fluid (Q) over total heat transfer area (A_h). The overall convective heat-transfer coefficient h_{avg} , and average Nusselt number Nu , were evaluated using the following equations (Eqs. 2 and 3)

$$h_{\text{avg}} = \frac{Q}{A_h \times \left[\frac{(T_w - T_{\text{in}}) - (T_w - T_{\text{out}})}{\ln \left(\frac{T_w - T_{\text{in}}}{T_w - T_{\text{out}}} \right)} \right]} \quad (2)$$

$$Nu = h_{\text{avg}} \times \frac{d}{k} \quad (3)$$

Total pumping power per serpentine was calculated from the pressure drop as:

$$\text{Pumping power (PP)} = \text{Pressure drop } (\Delta P) \times \text{Volumetric flow rate } (Q_f) \quad (4)$$

For the purpose of comparison, numerical simulations were also carried out for the case of straight channel having similar

Table 1. Summary of Literature Studies

No:	Authors	Details	Remarks
1	Chintada et al. ³	Numerical study; CS: square Re : 50 to 200; Pr : 0.7 to 7 $A/d_h = 0.5$ to 2; $DIPS/d_h = 0.5$ to 2	Heat transfer performance of serpentine channels was found to be better than that for straight channels for $Pr = 7.0$ and was worse than the straight channels for $Pr = 0.7$.
2	Maharudrayya et al. ⁴	Numerical study; CS: rectangular Re : 0.7 to 2300; Pr : 0.7 Sharp and smooth bends Rc/d_h : 0 to 6; 90° and 180° bend; α : 1 to 6	Presented correlations to predict excess bend coefficient as a function of Re, curvature ratio, aspect ratio, and the space length between the bends. Application of this correlation to typical fuel cell configurations showed significant contribution of bend loss to overall pressure loss especially for $Re > 1000$. Concluded that significant scope exists for the optimization of the channel configuration to achieve a desired pressure drop.
3	Rosaguti et al. ⁵	α : aspect ratio, width/height Numerical study; CS: circular Re: 0 to 200; Pr : 6.13 L_{half}/d_p : 4.5; Rc/d_h : 1	Observed enhancement in heat transfer and reduction in pressure drop with increase in L_{half}/d for $Rc/d_h = 1$ and $Pr = 6.13$.
4	Rosaguti et al. ⁶	Numerical study; CS: circular Re: 0 to 200; Pr : 0.7 to 100 L_{half}/d_h : 3.5 to 12.5; Rc/d_h : 0.525 to 2.25	Flow becomes unsteady for Re above 200. Reported significant heat transfer enhancements relative to flow in straight pipe with the greater effect at higher Pr .
5	Geyer et al. ⁷	Numerical study; CS: square Re: 0 to 200; Pr : 0.7 to 100 L_{half}/d_h : 3.6 to 12; Rc/d_h : 0.525 to 2	The results showed that heat transfer enhances with increase in Re with relatively small pressure drop penalty. The heat transfer enhancement reduces with reduction in the curvature ratio.
6	Rosaguti et al. ⁸	Numerical study; CS: semicircular Re: 0 to 450; Pr : 0.7 to 100 L_{half}/d_p : 3 to 12.5; Rc/d_p : 0.525 to 2.25	The authors observed that, for constant Re, increasing L_{half}/d_p and Rc/d_p decrease heat transfer enhancement as well as the pressure drop penalty.
7	Hsieh and Her ⁹	Numerical study; CS: rectangular Re: 10 to 421.4; 90° bend Fluid: methanol; d_h : 240 μ m	Reported variation of average Nu and friction factor with the Pe . Developed correlation based on their simulations to predict average Nu and f as a function of Pe and Re, respectively.
8	Xiong and Chung ¹²	Experimental study; CS: rectangular Re: 50 to 2300; Pr : 6.13 d_h : 0.209, 0.395, 0.549 mm	Evaluated bend loss coefficient for serpentine channel. Additional pressure drop due to serpentine was found to increase sharply for $Re > 100$. The bend loss coefficient was observed to decrease and tend to be a constant with decreasing Re.
9	Geyer et al. ¹⁰	Numerical study; CS: semicircular Re: 0 to 400; Pr : 6.13 L_{half}/d_p : 3.6 to 12; Rc/d_p : 0.525 to 1.3 B/L_{half} : 0.17 to 1, A/L_{half} : 0.125 to 1	The authors observed that swept zigzag pathway provides the greatest intensification of heat transfer in a multichannel plate structure.
10	Roasguti et al. ¹¹	Numerical study; CS: circular/ semicircular Re: 5 to 200; Pr : 6.13 L_{half}/d_p : 4.5, A/L_{half} : 0.222 to 0.667	The authors found that heat transfer enhancement exceeds the relative pressure-drop penalty by factors as large as 1.5 and 1.8 for the circular and semicircular cross-sections, respectively.

CS: cross-section, L_{half} : half wavelength of serpentine, Rc : radius of curvature/mean radius of bend; A : Amplitude of serpentine, d : passage dimension, $DIPS$: distance between inner of channel, d_h : hydraulic diameter, d_p : passage diameter of semicircle $d_h = \frac{\pi}{\pi+2}d_p$, B : length of the short side of the trapezoid.

dimensions as that of serpentine channel under the conditions of thermally developing flow. In this case, the inlet boundary condition for the momentum equation consists of a developed velocity profile for the channel aspect ratio of 1.5 with all four walls supplying heat to fluid. The rest of the simulation methodology was similar to that discussed above.

Experimental Setup and Procedure

Test piece

The experimental test piece consisted of a copper block having dimensions of $34 \times 30 \times 5$ mm³. On this block, a serpentine channel comprising of 10 bends in series were machined on one side using milling technique. The dimensions of single serpentine bend were 1 mm wide and 1.5 mm deep, and 46.28 mm in length. Figure 3a shows the image of the serpentine plate. The top portion of the plate was closed by 8-mm thick acrylic plate which was provided with 1 mm holes for arrangement of stainless steel needles to measure pressure as well temperature. Figure 3b shows the schematic of the pressure and temperature measurement locations. For inlet and outlet, 1 mm stainless steel needles were fitted at the ends. For heat transfer studies, the test piece was heated using A.C. strip heater with power/heat input controlled by the dimmerstat. The power supplied to

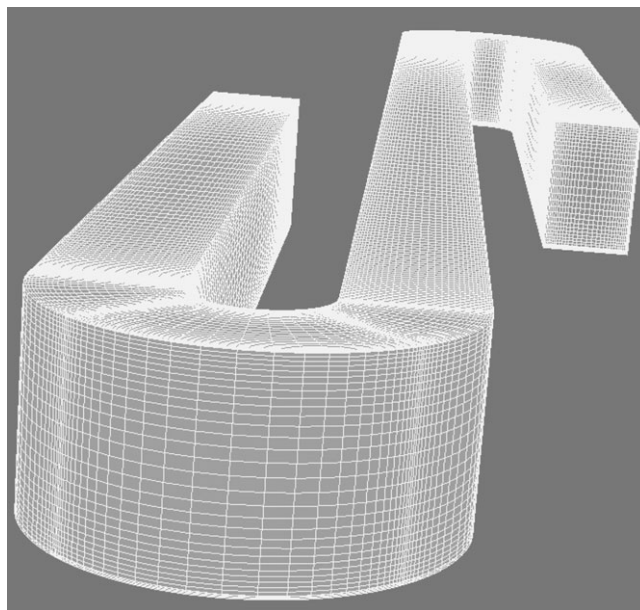


Figure 2. Computational domain (similar to as used in experimental section).

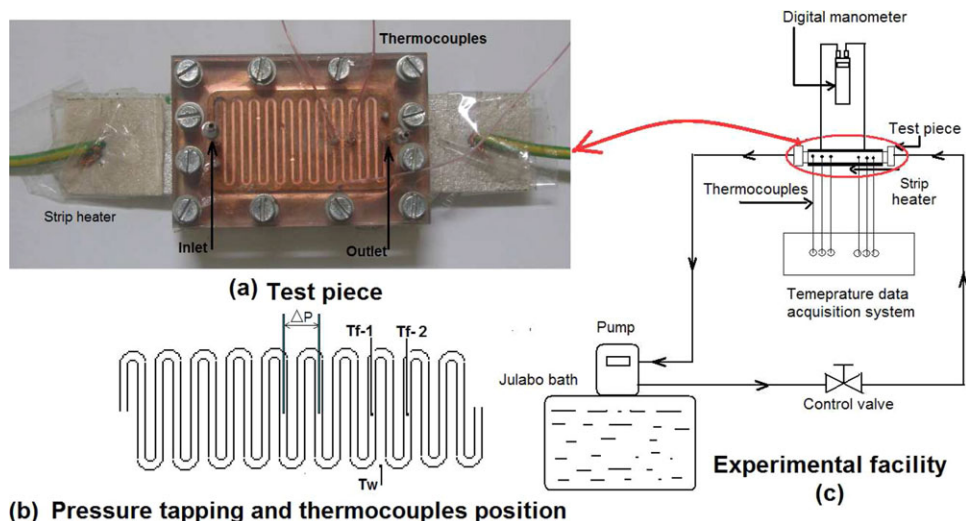


Figure 3. Experimental facility and test piece.

[Color figure can be viewed in the online issue, which is available at wileyonlinelibrary.com]

strip heater was measured by digital Wattmeter (Conserve model No: ELF3234, True RMS, one second update time, Accuracy: Class 1 .0 as per IEC 62052-11 and IEC 62053-21 i.e., $\pm 1\%$ of full-scale reading). The thermocouples of size 0.12 mm were placed inside channel and at copper surface to measure the temperature of the channel fluid as well as channel wall as shown in Figures 3a, b.

Measurement apparatus and procedures

The fluid was pumped using the pump provided on the standard Julabo bath. The flow through the geometry was controlled by using the control valve. The flow rates used in this study were in the range of 10 mL/min ($\sim \text{Re } 133$) to 50 mL/min ($\sim \text{Re } 666$) that was measured by collecting the volume of liquid in specific time. Figure 3c shows the schematic of the experimental setup. For pressure drop measurements, two holes of diameter 1 mm were drilled on the top polycarbonate cover exactly on the top of the channel with 46.28-mm axial distance (i.e., total length of single serpentine unit) between them. By this way, the pressure drop over only single serpentine unit was measured. Through these holes, two SS tubes/needles having internal diameter of 0.8 mm were inserted so as to make tube inline with the top surface of the channel. These two tubes were connected to the digital manometer having sensitivity of 7 Pa and accuracy of $\pm 0.3\%$ of full scale. Frictional pressure drop over the 46.28 mm length was directly measured by the digital manometer. For pressure drop measurement, serpentine bend near the outlet was selected to avoid entrance effects. It was assumed that latter units of serpentine bends represent periodic cases, that is, fully developed flow. For heat transfer studies, temperatures were recorded using data acquisition system at scanning rate of 1 s within accuracy of $\pm 0.5^\circ\text{C}$. Two thermocouples (Omega, T Type, Accuracy: $\pm 0.5^\circ\text{C}$) of size 0.076 mm were placed on the serpentine channel wall/fin to measure the wall temperature along the length of the channel. The water temperature in the single serpentine channel was measured by using two thermocouples placed in a channel so as to get information about the heat transferred to the water in a region of single serpentine bend. For testing procedure, the A.C. electrical power to the heater was adjusted to a desired level by a variable voltage of the dimmerstat.

After allowing the system to establish steady state, flow rate and temperatures were measured.

Data reduction

The collected pressure drop data were used to calculate effective friction factor as

$$\Delta P = \frac{2 f L_T \rho V^2}{D_h} \quad (5)$$

The Poiseuille number ($f\text{Re}$) was then calculated from friction factor (f) and Reynolds number (Re) as

$$f\text{Re} = \frac{\Delta P D_h}{2 L_T \rho V^2} \text{Re} \quad (6)$$

f and $f\text{Re}$ used in Eqs. 5 and 6 were friction factor and Poiseuille number for periodically developed flow.

The total energy given by the strip heater was partly supplied to water ($Q1$) and partly lost to environment ($Q2$). The heat taken by the water was calculated as

$$Q1 = \dot{M} C_p (T_{f,\text{out}} - T_{f,\text{in}}) \quad (7)$$

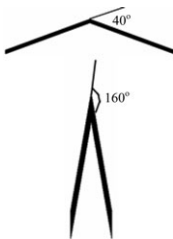
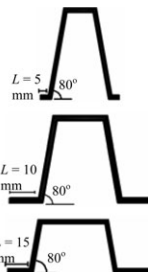
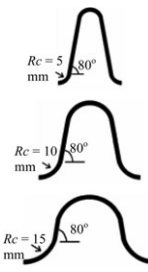
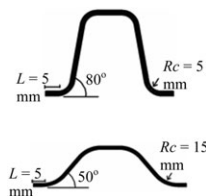
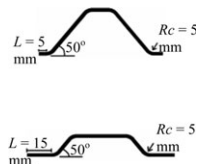
The heat loss to the environment was calculated using the difference between the heat supplied which was measured by the Wattmeter and total heat taken by water. The overall heat loss to the environment was found to be less than 10%. More than 100 temperature data points were used in calculations for every flow rate. The overall heat-transfer coefficient was calculated as

$$q1 = \frac{Q1}{(W \times L + 2 \times H \times L)_{\text{single serpentine}}} = h \times \left(\frac{(T_{w,\text{in}} - T_{f,\text{in}}) - (T_{w,\text{out}} - T_{f,\text{out}})}{\ln \left(\frac{T_{w,\text{in}} - T_{f,\text{in}}}{T_{w,\text{out}} - T_{f,\text{out}}} \right)} \right) \quad (8)$$

The mean Nusselt number was calculated as

$$Nu = \frac{h_{\text{avg}} D_h}{k} \quad (9)$$

Table 2. Different Geometrical Parameters of Serpentine Channel

Case 1: Effect of Inclination/Bending Angle (θ)	Case 2: Effect of Straight Length Before Bend (L)	Case 3: Effect of Radius of Curvature (R_c)	Case 4: Effect of Radius of Curvature When Length Before Bend is Constant	Case 5: Effect of Length Before Bend When Radius of Curvature is Constant
θ : 20–160° — e.g.,	θ : 20–90° L : 5–15 mm — e.g.,	θ : 40–160° — R_c : 5–20 mm e.g.,	θ : 20–90° L : 5 mm R_c : 5–20 mm e.g.,	θ : 20–90° L : 5–15 mm R_c : 5 mm e.g.,
				

Note: For case 3, the bending angle is twice of that shown in Table 1 i.e. in the example shown in table; the actual bending angle is 160°. Please refer Appendix II–Case 3 for detailed explanation.

CFD Simulations: Influence of Geometrical Parameters

Computational methodology

In the present work, periodic serpentine geometry consists of a square channel of $2 \times 2 \text{ mm}^2$ in cross section with periodic length of 100 mm. The effect of bend angle (θ), straight length before bend (L) (i.e., distance between the bends/2), and radius of curvature (R_c) on overall heat transfer enhancement over a straight channel was studied. The ranges of the parameters used in this study are given in Table 2. Total length of all of the serpentine configurations listed in Table 2 was kept constant at 100 mm. Under such condition, amplitude of the serpentine can be calculated (for a specified

angle) using the constraint on total length (see Appendix A). The computational domain for one of the serpentine configuration of Case 3 is shown in Figure 4.

The entire domain was meshed using hexahedral map elements. Grid sensitivity analysis was carried out and a computational grid of $30 \times 30 \times 720$ cells (single periodic serpentine) was found to be an appropriate choice. The channel width and height was meshed with double successive ratio of 1.1, whereas channel length was meshed with a double successive ratio of 1.02. Total 648,000 cells were used in simulation. The rest of the simulation procedure was same as mentioned earlier. Following four criteria were used to compare or analyze the influence of various geometrical parameters of serpentine channel.

Criteria 1	Criteria 2	Criteria 3	Criteria 4
$\frac{(PP)_{\text{Serpentine}}}{(PP)_{\text{straight channel}}}$	$\frac{(Q)_{\text{serpentine}}}{(Q)_{\text{straight channel}}}$	$\frac{(Q/PP)_{\text{serpentine}}}{(Q/PP)_{\text{straight channel}}}$	$\frac{(Nu/fRe)_{\text{Serpentine}}}{(Nu/fRe)_{\text{straight channel}}}$

where, Q : heat transferred, PP : pumping power.

Results and Discussion

Evaluation of CFD methodology with experimental data

Simulated values of Poiseuille number are compared with the experimental data in Figure 5a. Theoretical values of Poiseuille number (14.74^{13}) for fully developed flow in case of straight channel are also shown for comparison. It can be seen that the pressure drop for serpentine channel is higher than that of straight channel and the difference increases with increase in the value of Re (the serpentine channel pressure drop is around 1.2 times of straight channel at $Re = 130$. The same increases to around 1.9 times at $Re = 666$). The simulated values of Poiseuille number agree reasonably with the experimental data. Simulated values of Nusselt number as a function of Re for serpentine channel are shown in Figure 5b. The theoretical Nusselt number for

fully developed flow in case of straight channel (3.12^{13} for the case when all four walls are supplying heat) is also shown for comparison. It can be seen from Figure 5b that the simulated values of Nusselt number agree reasonably with the experimental data. Similar to the observation in pressure drop, the Nusselt number for serpentine channel is higher than that of straight channel and the difference increases with Re . As discussed earlier, the presence of secondary flow structures disrupts the thermal boundary layer at bends that results in better performance in terms of heat transfer. The Nusselt number for serpentine channel is around 1.9 times of straight channel for $Re = 130$ which increases to 4.32 times that of straight channel for $Re = 666$. Simulated values of Nusselt number for thermally developing flow in straight channel with same dimensions and operating conditions are also shown in Figure 5b. After establishing that CFD simulations agree reasonably with the experimental data, CFD simulations were used to investigate

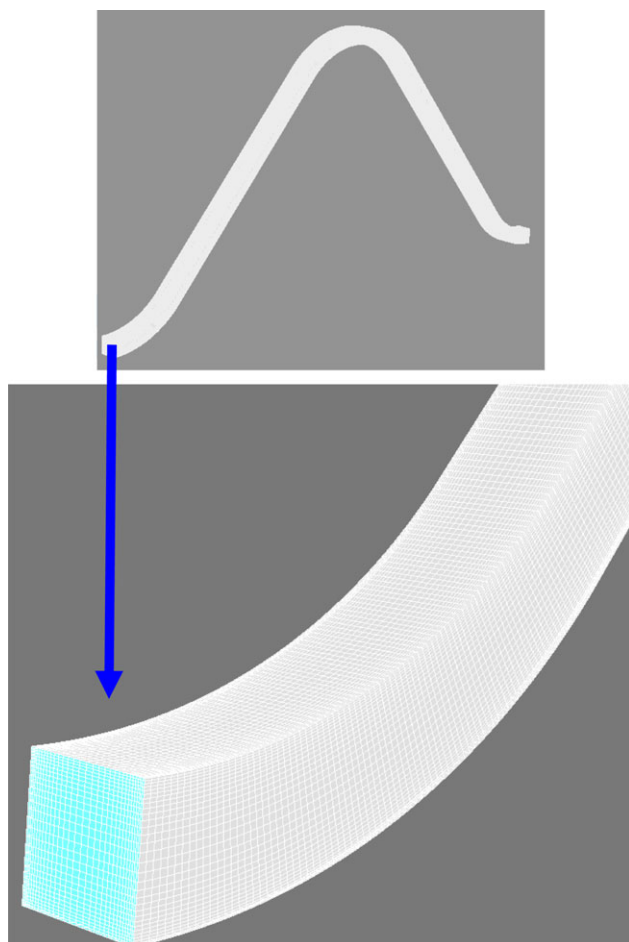


Figure 4. Example of computational domain used to study the effect of geometrical parameters of serpentine channel.

[Color figure can be viewed in the online issue, which is available at wileyonlinelibrary.com]

influence of different geometrical parameters on the performance of serpentine channel. These results are discussed in the following.

Effect of inclination/bend angle (θ) on performance

Influence of bend angle of serpentine channel (see Table 2) was studied. For these cases, the serpentine configuration was zigzag (saw tooth-like; see Appendix A or Table 2) with sharp bends. Simulated results are summarized in Figures 6a–d in terms of pumping power, heat transferred, heat transferred per unit pumping power, and Nu/fRe , respectively. All the results were obtained for Re equal to 200. All values were normalized with the results of the straight channel with same Re , length, aspect ratio, and cross sectional area.

It can be seen from the results that as expected the pumping power increases with increase in the bend angle (Figure 6a). The rate of increase of pressure drop with bend angle significantly reduces when bend angle increases beyond 90° . The enhancement in heat transfer increases with the bend angle till 90° (Figure 6b). Beyond this, contrary to the observation in case of pressure drop, further increase in bend angle reduces effective heat-transfer (coefficient). This may be because of the dead zones developed at the bend corner for higher bend angle geometries (see e.g., velocity contour plots for different bend angles shown in Figure 7). The maximum heat transfer enhancement is obtained for the serpentine configurations having bend angle of 90° . From the overall result, it can be seen that the configurations with 50 – 90° bend angle give better result in terms of heat transferred per unit pumping power by Criterion 3 (Figure 6c) as well as by Criterion 4 (Figure 6d).

Effect of straight length (L) before bend on performance

In the second case (refer Table 2), influence of straight length before bend was studied. The difference between the Case 1 and the present case is that the sharp bends used in the Case 1 were separated by the straight portions between them. The simulated results for this case are summarized in Figures 8a–d. Results obtained for Case 1 ($L = 0$) are also shown in Figure 8 to facilitate comparison.

It can be seen from the results that for all angles, the pressure drop and heat transfer enhancement in the present case is more than that of Case 1. Typically, the pumping power and heat transfer enhancement increase with increase in

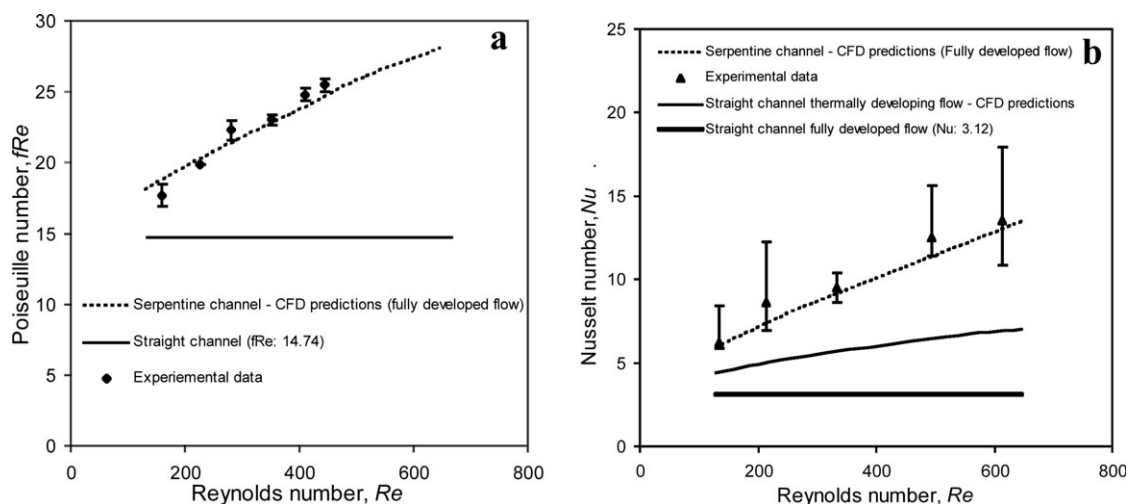


Figure 5. Comparison between experimental data and CFD simulation.

(a) Poiseuille number in serpentine channel (b) Nusselt number in serpentine channel.

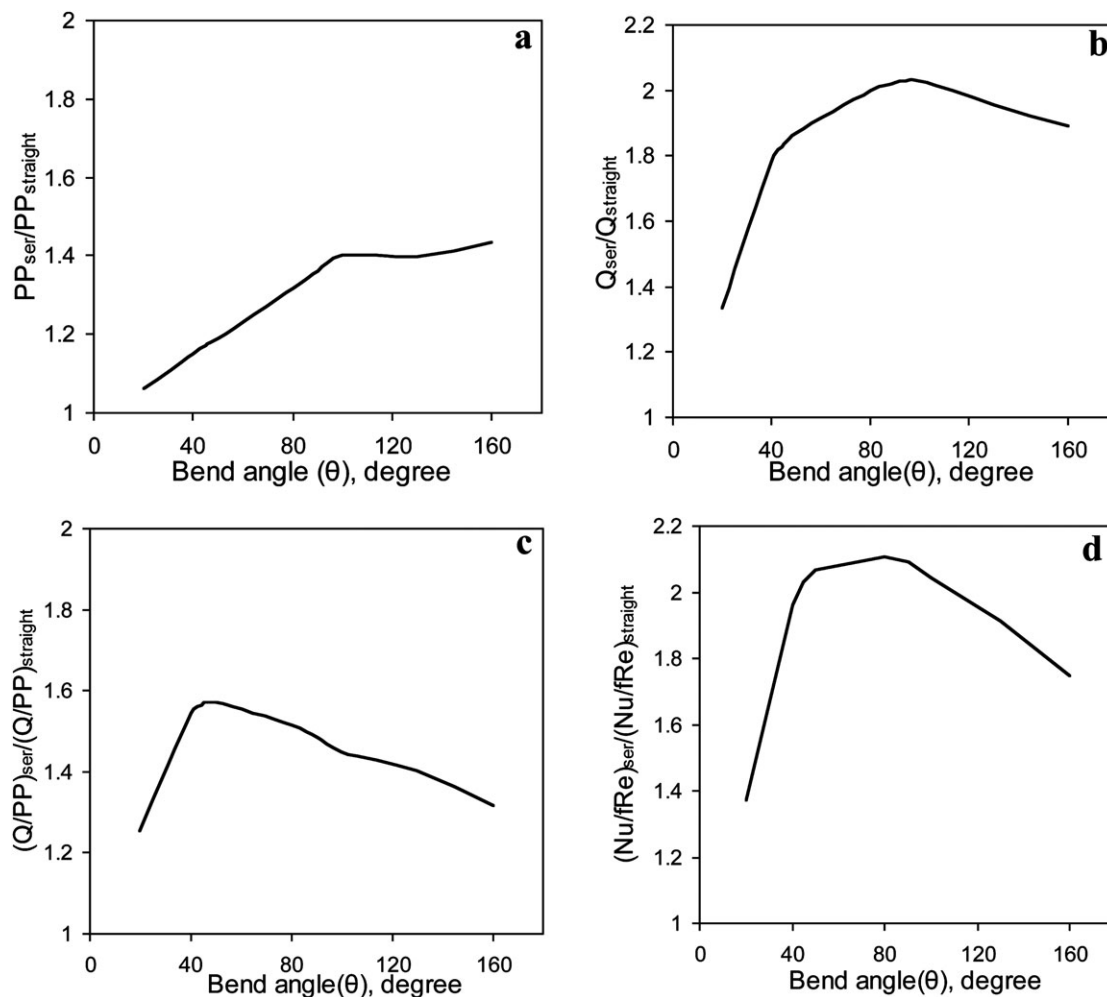


Figure 6. Case 1—effect of bend angle on (a) pumping power (b) heat transfer enhancement (c) heat transfer per unit pumping power (d) Nu/fRe .

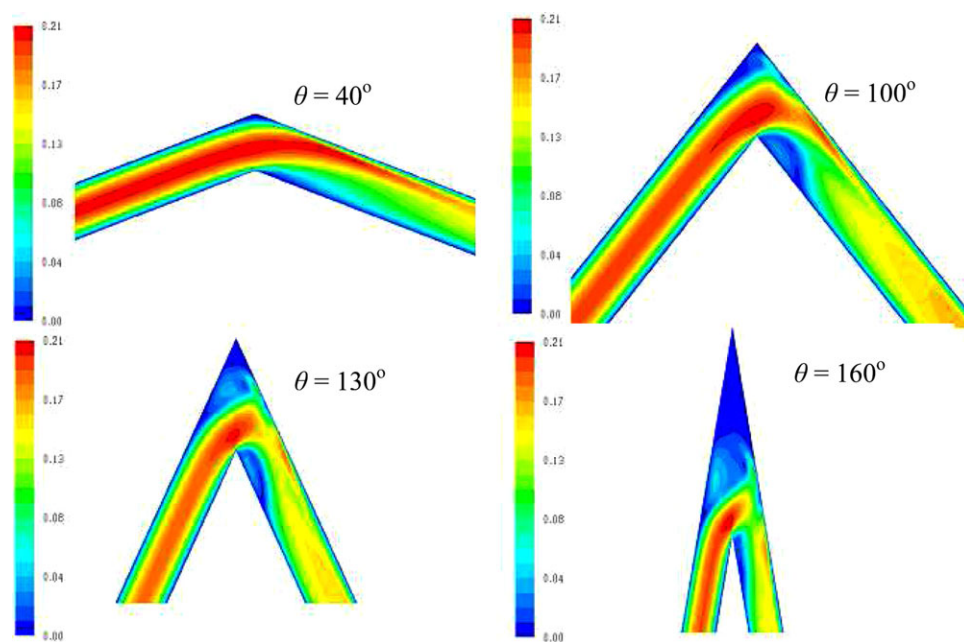


Figure 7. Velocity contour plot for different bend angles ($Re = 200$; middle plane).

[Color figure can be viewed in the online issue, which is available at wileyonlinelibrary.com]

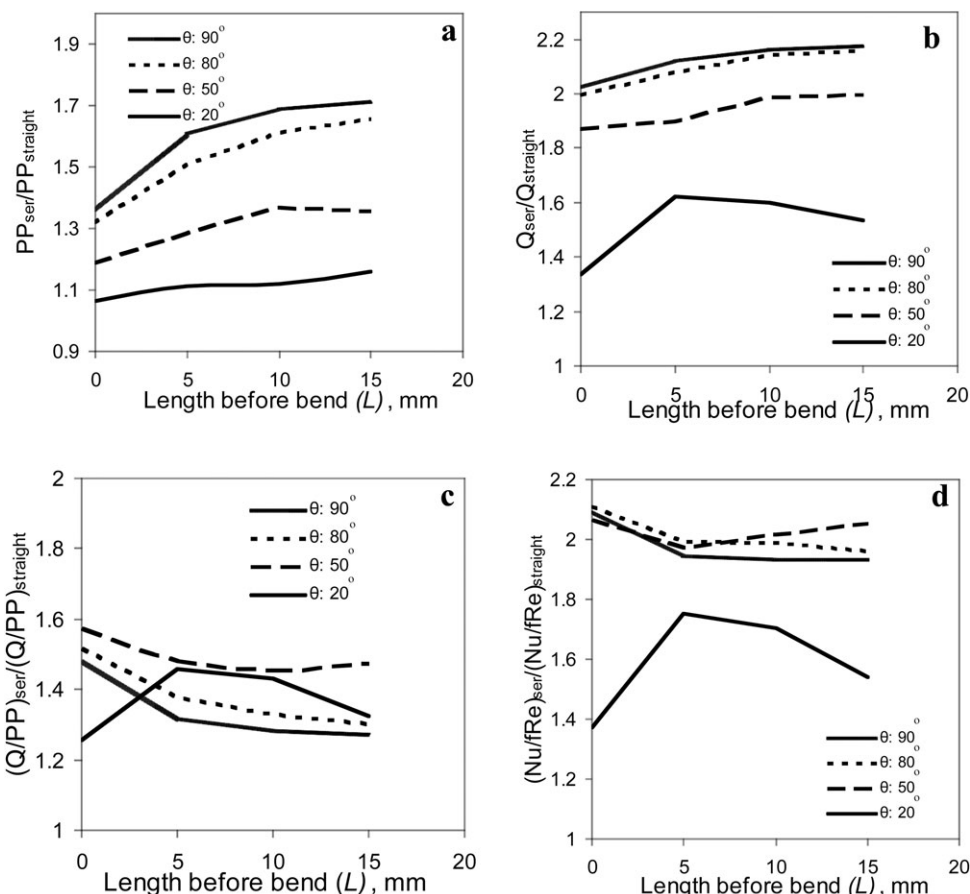


Figure 8. Case 2—effect of straight length before bend in sharp bends or in absence of curvature on (a) pumping power (b) heat transfer enhancement (c) heat transfer per unit pumping power (d) Nu/Re .

length before the bend in all the cases except for serpentine configurations having small bend angles, that is, 20° . In this case, contrary to the observation of pressure drop, further increase in straight length reduces effective heat-transfer (coefficient). In case of small length (i.e., 5 mm), the distance between the second and the third bend is small (case of 20°) and together both create good radial mixing (i.e., better temperature homogenization) when placed closed to each other.

The pumping power in serpentine configurations of Case 2 (particularly $\theta > 20^\circ$) is also governed by the flow development length/hydrodynamic development length after the bend. Therefore, as the straight portion (L) before the bend increases, the overall portion of the continuous straight length reduces (i.e., decrease in amplitude or decrease in distance between the 1st and 2nd bend). Part of the flow remains in developing region. Therefore, the heat transfer enhancement increases with increase in length of the straight portion before the bend (Figure 8b). A sample of disruption in velocity profile caused by a sharp bend (of Case 2) is shown Figures B1, B2 in Appendix B.

The ratio of heat transfer rate divided by pumping power of serpentine channel to that of straight channel is highest for 50° bend angle serpentine configuration (Figure 8c), whereas highest heat transfer is obtained for 90° bend angle configuration (Figure 8b). The Criterion 3 indicates that the 50° bend angle gives the best result, whereas the Criterion 4 indicates that (Figure 8d) configurations with bend angle above 50° are better.

Effect of curvature (R_c) on performance

In the third case (refer Table 2), influence of radius of curvature of the bend was studied. The results are summarized in Figures 9a–d. Along with these results, the results of serpentine with sharp bend (Case 1) or $R_c = L = 0$ are also shown in Figure 9.

For serpentine configurations where fluid was turned by higher angle, that is, 100 – 160° , replacing sharp bend with curvature/smooth bend significantly decreases total pumping power (Figure 9a). Contrary to this, in case of 100 – 160° bend angle serpentine configuration, further increase (above 5 mm) in radius of curvature results in somewhat increased pressure drop due to increased total curved portion length. A sample of simulated flow results of smooth bends is shown in Figures 3–5 in Appendix B. As expected, the sharp bend creates somewhat better temperature homogenization (i.e., better heat-transfer coefficient) compared to smooth bend with requiring higher pumping power. The variations of radius of curvature (or degree of smoothness) for a given bend angle produces nearly same amount of boundary layer disruption (in the range studied) and, therefore, have insignificant effect on heat transfer enhancement (Figure 9b).

The highest enhancement is obtained for a serpentine configuration (with presence of curvature) having bend angle of 160° . It can be seen that this high bend angle serpentine configuration gives highest enhancement with lesser increase in pumping power (i.e., Case 3) than that of in the absence of

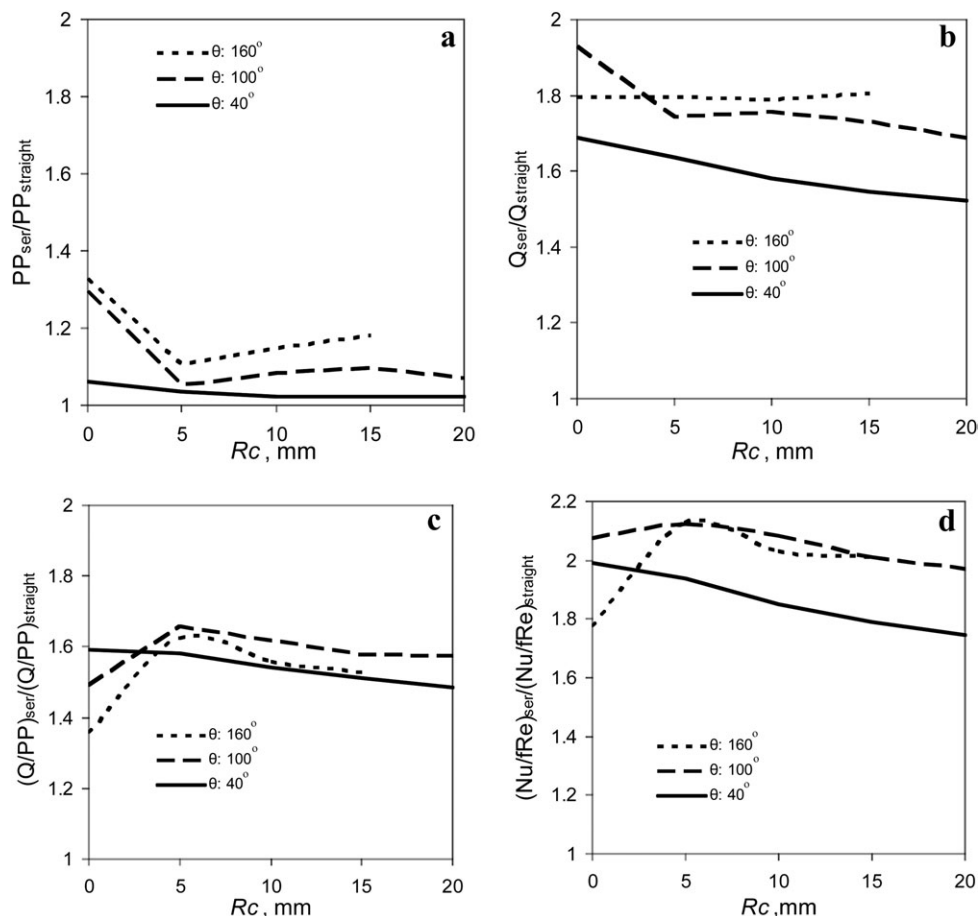


Figure 9. Case 3—effect of radius curvature in absence of straight length between bend on (a) pumping power (b) heat transfer enhancement (c) heat transfer per unit pumping power (d) Nu/fRe .

curvature (i.e., Case 1). Overall, higher bend angle geometries (100° and above) give better performance when compared as per Criteria 3 and 4 (Figures 9c, d).

Effect of curvature (R_c) with constant straight length before bend (L) on performance

Influence of radius of curvature (smoothness of a bend) keeping the straight length before bend (L) fixed at 5 mm was studied as Case 4 (refer Table 2). The results are summarized in Figures 10a–d. In this case, the sharp bend after the straight length of Case 2 is replaced by the curvature (i.e., sharp bend of Case 2 is replaced by smooth bend). Along with the effect of curvature (i.e., studies of Case 4), these figures also show the results of Case 2 for comparison (i.e., presence of sharp bends) with $L = 5$ and $R_c = 0$. It can be seen from Figures 10c, d that the serpentine configurations with bend angle above 50° show better performance. It can also be seen that the serpentine configurations which give higher heat transfer enhancement also show favorable heat transfer per unit pumping power (Q/PP). It is, therefore, possible to manipulate performance of serpentine channels by appropriate combination of curvature (R_c), straight length before bend (L), and bend angle (θ).

Effect of different straight length before bend (L) with constant curvature (R_c)

Influence of different straight length (L) before bend for the fixed radius of curvature (i.e., constant bend smoothness, R_c) of 5 mm was studied as Case 5 (see Table 2). The

results are summarized in Figures 11a–d. The results of Case 3 (with $L = 0$ and $R_c = 5$) are also shown in Figure 11 for comparison.

For serpentine configurations having low bend angle, for example, 20° , similar behavior as observed in Case 2 is seen, that is, no effect of increasing the straight length before the curvature on pumping power (Figure 11a) and increasing the heat transfer to certain extent (up to $L = 5$ mm) and then decreasing. As discussed in Case 2, for lower angle serpentine configurations, two closer bends (i.e., case of smaller length before bends) result in better heat transfer enhancement (Figure 11b). Increasing this length above certain value ($L = 10$ mm), however, resulted in decrease in heat transfer enhancement. For serpentine configurations having higher bend angle, for example, 50° and above, straight length before curvature increases the pumping power to certain extent (up to L of about 5 mm). It should be noticed that influence of straight portion before bend and amplitude are always opposite to each other for a constant total length. Therefore, these two opposing effects result in only minor increase in heat transfer enhancement for serpentine configuration with 50° and above (for increase in straight length before bend from 5 to 15 mm, see Figure 11b). The serpentine configurations above 50° bending angle give quite favorable performances in terms of Q/PP and Nu/fRe (see Figure 11d).

Effect of bend angle (θ) for different Reynolds number

Influence of bend angle (i.e., Case 1) was investigated at two values of Re (200 and 50) to quantify influence of Re .

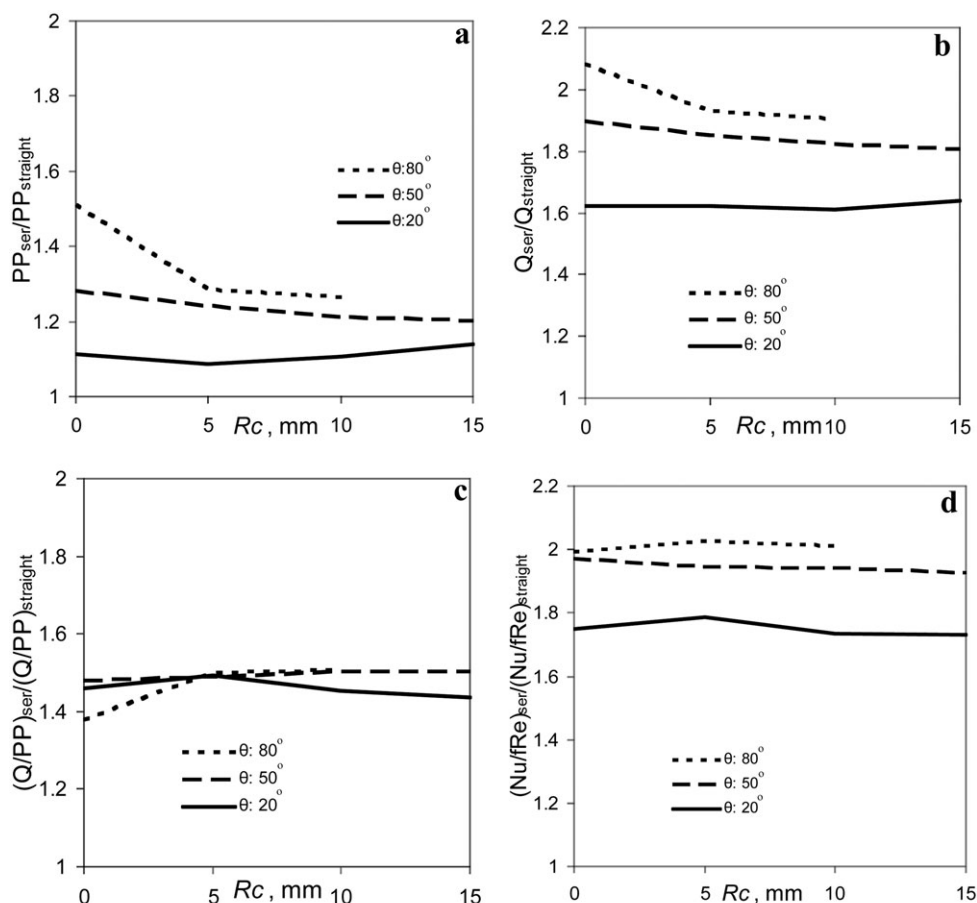


Figure 10. Case 4—effect of radius curvature for a fixed straight length before bend of 5 mm on (a) pumping power (b) heat transfer enhancement (c) heat transfer per unit pumping power (d) Nu/fRe .

These results are shown in Figure 12a–d. The ratio of pressure drop of serpentine channel to straight channel was found to increase with increase in bend angle for Re equal to 200 till angle of 100° . Beyond this angle, the ratio for Re equal to 200 was almost the same. Contrary to this, for Re equal to 50, this ratio was found to decrease with further increase in the bend angle. One of the possible reasons for this may be some differences in cross-section of channels at the bed at different bend angles. The highest heat transfer enhancement was achieved at 90° and 130° bend angle serpentine configuration for the value of Re equal to 200 and 50, respectively. (Figure 12b). Apparently, adequate boundary layer disruption (or temperature homogenization) is not achieved by lower bend angles in case of Re equal to 50. The 130° bend angle serpentine configuration is capable of achieving better boundary layer disruption, thus, giving highest heat transfer enhancement for the case of Re equal to 50 and, therefore, is better for this Re .

The mechanism of heat transfer enhancement in case of serpentine channel involves disruption of thermal boundary layer which ultimately depends on bend angle or curvature. The second governing parameter observed is distance between the bends. If the distance between the bends is higher, then the flow becomes fully developed before reaching the next bend (which may lower the performance). Based on the results discussed so far, a map of heat transfer enhancement vs. pumping power was generated to understand influence of various geometrical parameters for Re

200. This map is shown in Figure 13. It can be seen from the map that highest pumping requirement is 1.71 times that of the straight channel, whereas the highest heat transfer enhancement is up to 2.18 times that of the straight channel for the range of the serpentine configurations studied in the present work. Serpentine channels with smooth bends were found to realize better heat transfer enhancement (per unit pumping power) than those with the sharp bends. Overall, serpentine channels with a lower radius of curvature (i.e., $R_c = 5$ mm) and higher bend angle ($\theta = 80\text{--}160^\circ$) appear to be the best ($\sim 90\%$ enhancement in heat transfer is obtained with only about 20% higher pressure drop compared to the straight channel).

The results presented here are being extended to quantify influence of key parameters of serpentine channel on residence time distribution. These results will be useful for appropriate selection of serpentine channels for designing microreactors/ heat exchangers.

Conclusions

Flow and heat transfer in serpentine channels was investigated using CFD. A set of experiments were carried out to ensure that the developed CFD model adequately captures the reality. After establishing reasonable agreement of simulated results with the experimental data, CFD model was used to quantify influence of various geometrical parameters of serpentine channel (bend angle, straight length before bend, and curvature) on pressure drop and heat transfer (at a

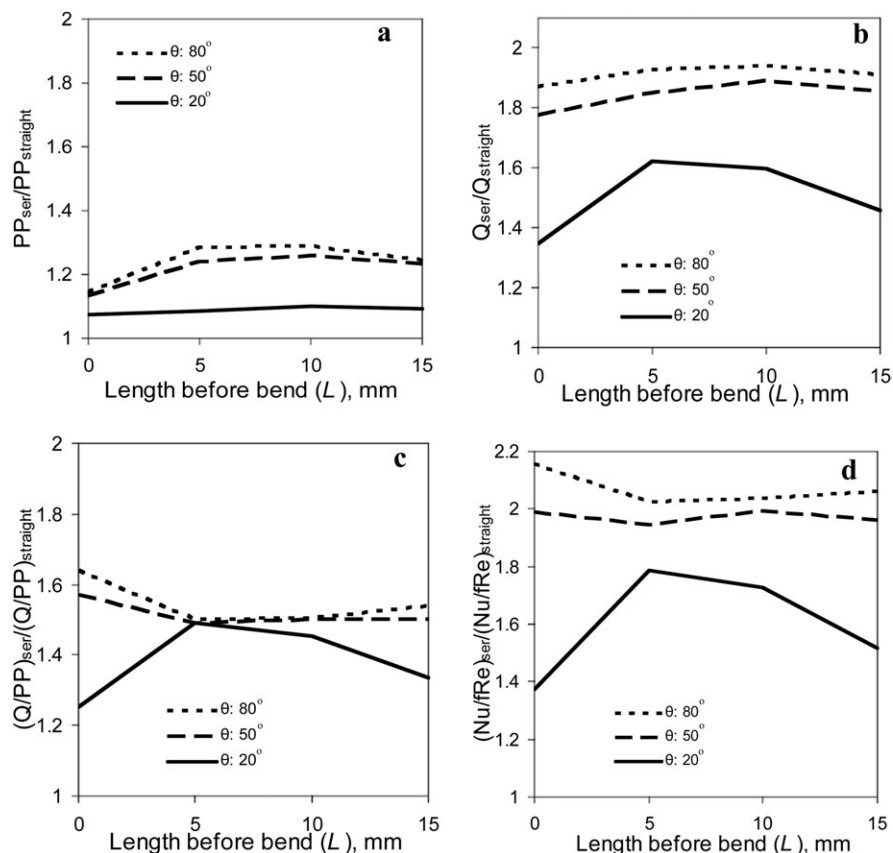


Figure 11. Case 5—effect of straight length before bend for a fixed curvature of 5 mm between the bend on (a) pumping power (b) heat transfer enhancement (c) heat transfer per unit pumping power (d) Nu/fRe .

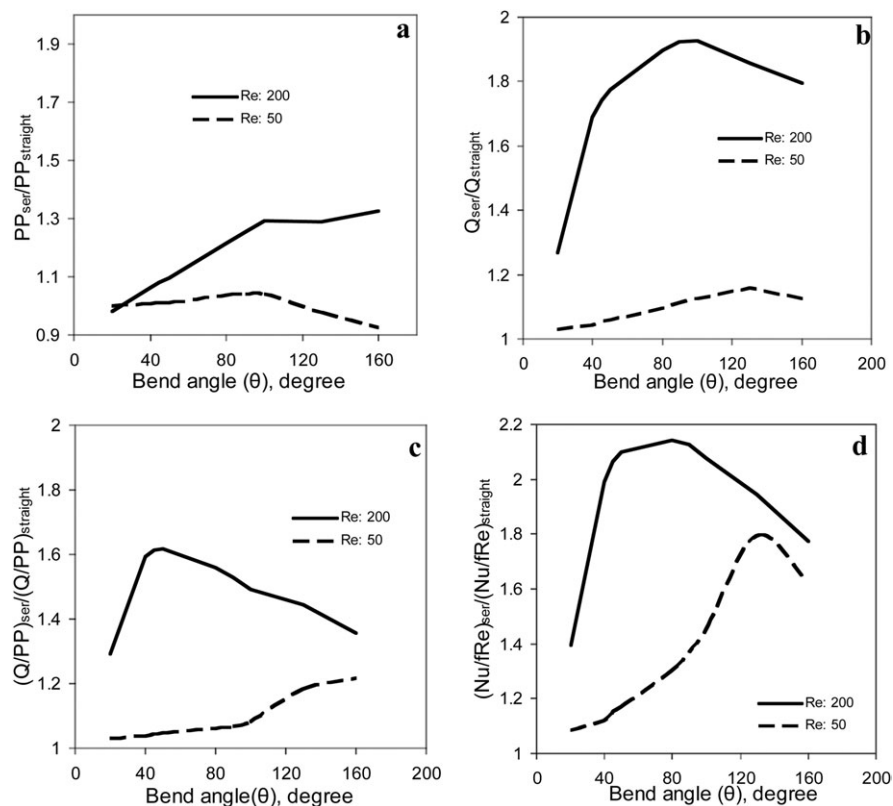


Figure 12. Effect of bend angle for different Re (a) pumping power (b) heat transfer enhancement (c) heat transfer per unit pumping power (d) Nu/fRe .

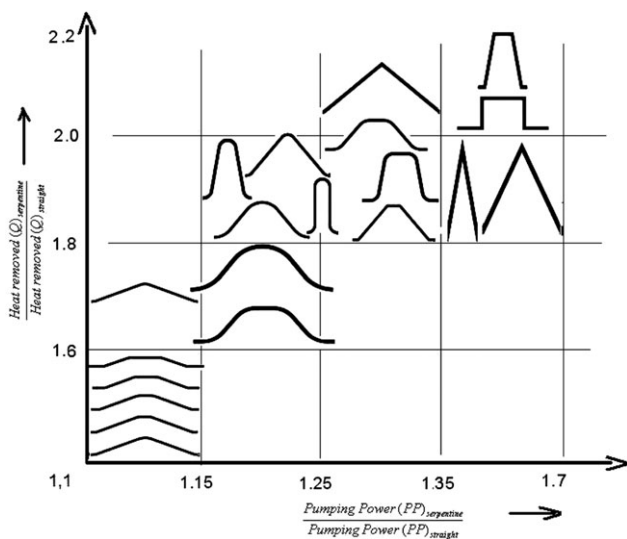


Figure 13. Design map of different serpentine configurations (Note: axis not to scale).

constant Re [200] and Pr [6.13]). Influence of $Reynolds$ number was quantified by carrying out simulations at Re equal to 50. Key conclusions obtained from the study are:

- Serpentine configurations with smooth bends offer lower pressure drop compared to those with sharp bends. Effect of variation of radius of curvature in case of smooth bend is found to be insignificant (in the range studied).

- Configuration showing highest heat transfer enhancement need not be the best when compared on the basis of unit pumping power. For example, for Cases 1 and 2 from Table 2 (cases with sharp bends, straight length before bends, and curvatures), the highest heat transfer enhancement was obtained for 90° bend angle. However, serpentine channel with 50° bend angle was found to be better when compared with unit pumping power basis.

- The optimal bend angle (based on heat transfer per unit pumping power) was found to be sensitive to the value of $Reynolds$ number. For example, 100° bend angle is optimum for $Re = 200$, whereas 130° bend angle is optimum for $Re = 50$.

Based on this work, a design map comprising different serpentine channels showing heat transfer enhancement with pumping power was developed for $Reynolds$ number of 200 which will be useful for further work on flow and heat transfer in serpentine channels. The results discussed here with appropriate extension to residence time distribution will be useful for appropriate selection of serpentine channels for designing microreactors/ heat exchangers.

Notation

A = amplitude of serpentine, m
 C_p = specific heat, J/kg K
 D_h = channel hydraulic diameter, m
 d, d_h = hydraulic diameter of serpentine channel, m
 f = friction factor, dimensionless
 fRe = Poiseuille number, dimensionless
 H = depth of channel, m
 h_{avg} = average heat-transfer coefficient, W/m^2K
 k = thermal conductivity of fluid, W/mk
 k_L = thermal conductivity of liquid, W/mk
 L_T = total length of channel, m

L = straight length before bend, m
 L_{half} = half wavelength of the serpentine path, m
 M = mass flow rate, kg/s
 Nu = average Nusselt number, dimensionless
 ΔP = pressure drop, N/m^2
 PP = pumping power, W
 $Q1$ = heat taken by fluid by convection, W
 $Q2$ = heat loss to environment, W
 Q_{ser} = heat transfer rate in serpentine channel, W
 Q = total heat transfer from the wall to fluid, W
 Rc = radius of curvature, m
 r = radius of channel, m
 Re = $Reynolds$ number, $(d u \rho / \mu)$, dimensionless
 $T_{f,out}$ = exit temperature of fluid from channel, K
 $T_{f,in}$ = inlet temperature of fluid to channel, K
 T_{in} = inlet fluid temperature of serpentine channel, K
 T_{out} = outlet fluid temperature of serpentine channel, K
 T_w = channel wall temperature, K
 V = mean axial velocity, m/s
 W = width of channel, m

Greek letters

ρ = density, kg/m^3
 μ = viscosity, $kg/(ms)$
 θ = angle of bend in serpentine, degree

Acronyms

A.C. = Alternate Current
 CFD = Computational Fluid Dynamics
 CHF = Constant Heat Flux
 IEC = International Electrotechnical Commission
 RMS = Root Mean Square
 SS = Stainless Steel

Subscripts and Superscripts

avg = average

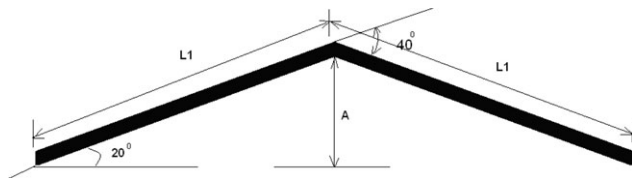
Literature Cited

- Jensen KF. Microreaction engineering is small better? *Chem Eng Sci.* 2001;56:293–303.
- Halder R, Lawal A, Damavarapu A. Nitration of toluene in micro-reactor. *Cataly Today.* 2007;125:74–80.
- Chintada S, Ko KH, Anand NK. Heat transfer in 3-D serpentine channels with right-angle turns. *Numer Heat Transf Part A: Appl Int J Comput Methodol.* 1999;36:781–806.
- Maharudrayya S, Jayanti S, Deshpande AP. Pressure losses in laminar flow through serpentine channels in fuel cell stacks. *J Power Sources.* 2004;138:1–13.
- Rosaguti NR, Fletcher DF, Haynes BS. Laminar flow in a periodic serpentine channel. In: *Proceedings of the 5th Australasian Fluid Mechanics Conference*, The University of Sydney, Sydney, Australia, 2004.
- Rosaguti NR, Fletcher DF, Haynes BS. Laminar flow and heat transfer in periodic serpentine channel. *Chem Eng Technol.* 2005;28: 353–361.
- Geyer PE, Rosaguti NR, Fletcher DF, Haynes BS. Thermohydraulics of square-section microchannels following a serpentine path. *Microfluid Nanofluid.* 2006;2:195–204.
- Rosaguti NR, Fletcher DF, Haynes BS. Laminar flow and heat transfer in a periodic serpentine channel with semi-circular cross-section. *Int J Heat Mass Transf.* 2006;49:2912–2923.
- Hsieh SS, Her BS. Heat transfer and pressure drop in serpentine IDMF flow channels. *Int J Heat Mass Transf.* 2007;50:5323–5327.
- Geyer PE, Fletcher DF, Haynes BS. Laminar flow and heat transfer in a periodic trapezoidal channel with semi-circular cross-section. *Int J Heat Mass Transf.* 2007;50:3471–3480.
- Rosaguti NR, Fletcher DF, Haynes BS. Low- $Reynolds$ number heat transfer enhancement in sinusoidal channels. *Chem Eng Sci.* 2007;62:694–702.
- Xiong R, Chung JN. Flow characteristics of water in straight and serpentine micro-channels with miter bends. *Exp Therm Fluid Sci.* 2007;31:805–812.
- Shah RK, London AL. *Laminar Flow Forced Convection in Ducts.* New York, San Francisco: Academic Press, London, 1978.

Appendix A: Dimensions of Serpentine Channel Configurations: Sample Calculation

Sample calculations of case 1

Bend Angle of 40°



Total Length: 100 mm

Straight length before bend (see Figure 1a for straight length definition): $L = 0$

Radius of curvature (Rc): 0

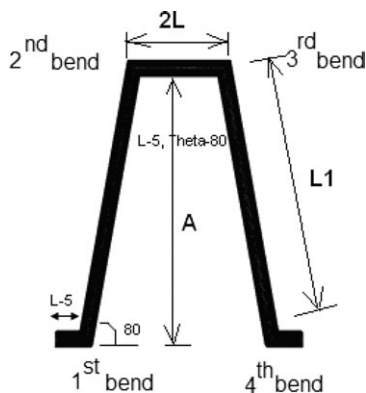
This makes $2 \times L1 = 100$ mm

i.e., $L1 = 50$ mm

$A = \sin(20) \times L1 = 17.101$ mm

Sample calculations of Case 2

Bend Angle of 80°



Total Length: 100 mm

Straight length before bend (see Figure 1a for straight length definition): $L = 5$ mm

Radius of curvature: 0

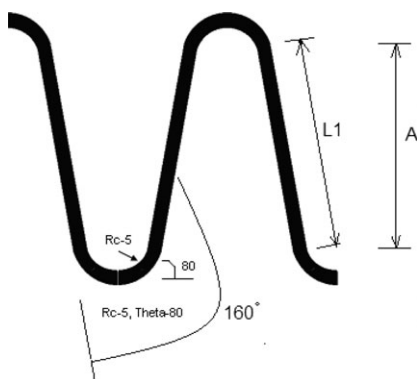
This makes $2 \times L1 + 2L + 2 \times L = 100$ mm

i.e., $L1 = 40$ mm

$A = \sin(80) \times L1 = 39.39$ mm

Sample calculations of Case 3

Bend Angle of 80°



Total Length: 100 mm

Straight length before bend (see Figure 1a for straight length definition): $L = 0$ mm

Radius of curvature (Rc): 5 mm

This makes $2 \times L1 + 4 \times Rc = 100$ mm

i.e., $L1 = 40$ mm

$A = \sin(80) \times L1 = 39.39$ mm

Appendix B: Supporting Data on Flow and Heat Transfer in Serpentine Channel ($Re = 200$)

Table B1. Case 1—Effect of Inclination/Bend Angle on Performance

θ Degrees	L (mm)	Rc (mm)	$PP_{Serpentine}$ $PP_{Straight\ channel}$	$Q_{Serpentine}$ $Q_{Straight\ channel}$	$Q/PP_{Serpentine}$ $Q/PP_{Straight\ channel}$	$Nu/f\ Re_{Serpentine}$ $Nu/f\ Re_{Straight\ channel}$
20	0	0	1.063	1.334	1.256	1.373
40	0	0	1.149	1.778	1.546	1.960
45	0	0	1.170	1.834	1.567	2.032
50	0	0	1.189	1.869	1.571	2.066
100	0	0	1.401	2.028	1.448	2.043
130	0	0	1.396	1.956	1.401	1.912
160	0	0	1.435	1.889	1.317	1.746

Table B2. Case 2—Effect of Straight Length (L) Before Bend on Performance

θ Degrees	L (mm)	Rc (mm)	$PP_{Serpentine}$ $PP_{Straight\ channel}$	$Q_{Serpentine}$ $Q_{Straight\ channel}$	$Q/PP_{Serpentine}$ $Q/PP_{Straight\ channel}$	$Nu/f\ Re_{Serpentine}$ $Nu/f\ Re_{Straight\ channel}$
20	5	0	1.112	1.624	1.459	1.750
20	10	0	1.119	1.601	1.430	1.702
20	15	0	1.1581	1.532	1.323	1.538
50	5	0	1.283	1.898	1.479	1.970
50	10	0	1.367	1.988	1.454	2.014
50	15	0	1.354	1.997	1.475	2.051
80	5	0	1.509	2.079	1.377	1.992
80	10	0	1.611	2.142	1.329	1.986
80	15	0	1.657	2.158	1.301	1.961
90	5	0	1.608	2.119	1.317	1.943
90	10	0	1.686	2.160	1.281	1.932
90	15	0	1.711	2.175	1.270	1.932

Table B3. Case 3—Effect of Curvature on Performance

θ Degrees	L (mm)	Rc (mm)	$PP_{Serpentine}$ $PP_{Straight\ channel}$	$Q_{Serpentine}$ $Q_{Straight\ channel}$	$Q/PP_{Serpentine}$ $Q/PP_{Straight\ channel}$	$Nu/f\ Re_{Serpentine}$ $Nu/f\ Re_{Straight\ channel}$
40	0	5	1.121	1.721	1.535	1.906
40	0	10	1.109	1.662	1.497	1.820
40	0	15	1.108	1.626	1.467	1.760
40	0	20	1.109	1.601	1.443	1.717
100	0	5	1.051	1.835	1.139	2.088
100	0	10	1.084	1.847	1.175	2.049
100	0	15	1.095	1.820	1.186	1.977
100	0	20	1.072	1.778	1.162	1.940
160	0	5	1.199	1.890	1.576	2.0914
160	0	10	1.246	1.883	1.511	1.999
160	0	15	1.280	1.900	1.483	1.976

Table B4. Case 4—Effect of Curvature with Constant Straight Length Before Bend on Performance

θ Degrees	L (mm)	Rc (mm)	$PP_{Serpentine}$ $PP_{Straight\ channel}$	$Q_{Serpentine}$ $Q_{Straight\ channel}$	$Q/PP_{Serpentine}$ $Q/PP_{Straight\ channel}$	$Nu/f\ Re_{Serpentine}$ $Nu/f\ Re_{Straight\ channel}$
20	5	5	1.086	1.6210	1.492	1.787
20	5	10	1.107	1.609	1.453	1.733
20	5	15	1.140	1.638	1.437	1.731
50	5	5	1.241	1.850	1.490	1.945
50	5	10	1.210	1.821	1.504	1.940
50	5	15	1.200	1.805	1.504	1.928
80	5	5	1.509	2.079	1.377	1.992
80	5	10	1.285	1.930	1.500	2.025

Table B5. Case 5—Effect of Different Straight Length Before Bend with Constant Curvature on Performance

θ	L	R_c	$PP_{Serpentine}$	$Q_{Serpentine}$	$Q/PP_{Serpentine}$	$Nu/f Re_{Serpentine}$
Degrees (mm)	(mm)	(mm)	$PP_{Straight\ channel}$	$Q_{Straight\ channel}$	$Q/PP_{Straight\ channel}$	$Nu/f Re_{Straight\ channel}$
20	5	5	1.086	1.621	1.492	1.787
20	10	5	1.100	1.598	1.452	1.726
20	15	5	1.090	1.456	1.335	1.515
50	5	5	1.145	1.850	1.241	1.945
50	10	5	1.162	1.891	1.259	1.993
50	15	5	1.137	1.852	1.232	1.963
80	5	5	1.285	1.930	1.500	2.025
80	10	5	1.289	1.940	1.504	2.038
80	15	5	1.243	1.913	1.538	2.061

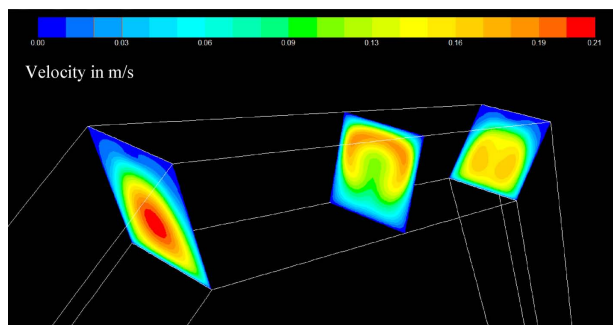


Figure B1. Velocity contours at few planes in bend region in Case 2, that is, presence of straight length before bend (L : 5 mm, θ : 50°).
[Color figure can be viewed in the online issue, which is available at wileyonlinelibrary.com.]

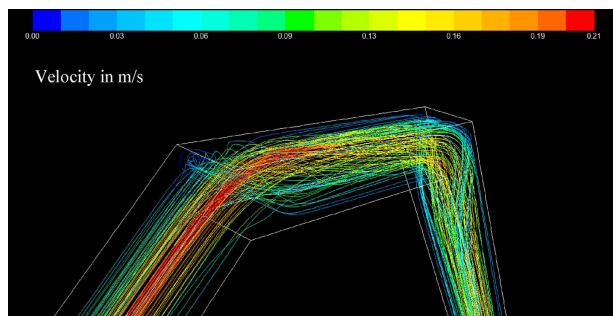


Figure B2. Path lines at bend region in Case 2, that is, presence of straight length before bend (L : 5 mm, θ : 50°).
[Color figure can be viewed in the online issue, which is available at wileyonlinelibrary.com.]

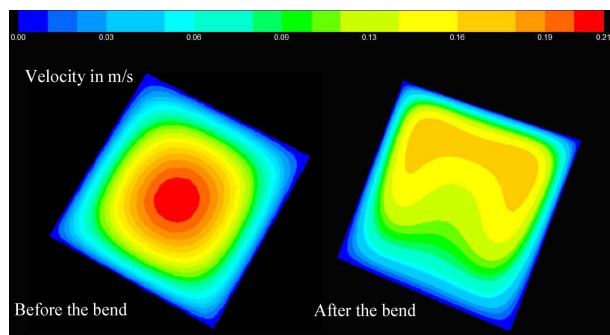


Figure B3. Velocity contours in case of 5 mm radius of curvature with 100° bend angle, that is, Case 3.

[Color figure can be viewed in the online issue, which is available at wileyonlinelibrary.com.]

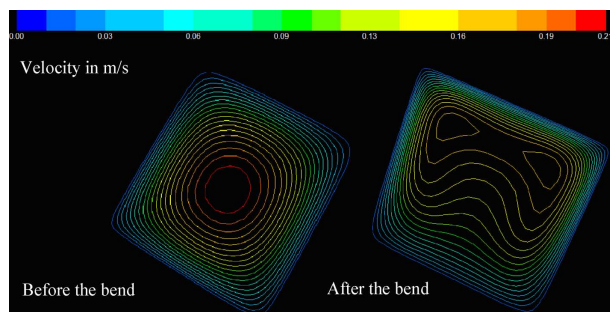


Figure B4. Velocity contour lines in case of 5 mm radius of curvature with 100° bend angle, that is, Case 3.

[Color figure can be viewed in the online issue, which is available at wileyonlinelibrary.com.]

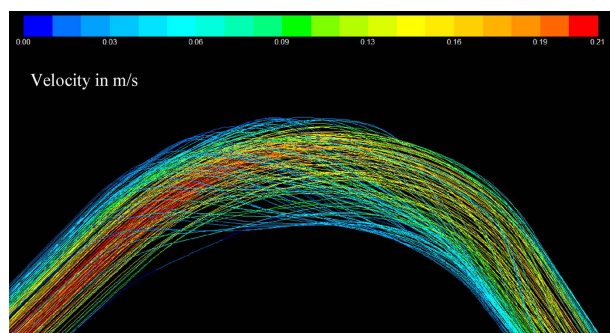


Figure B5. Path lines in case of 5 mm radius of curvature with 100° bend angle, that is, Case 3.
[Color figure can be viewed in the online issue, which is available at wileyonlinelibrary.com.]

Manuscript received Jan. 8, 2012, and revision received Sept. 25, 2012.